

# GRASP: Guided Region-Aware Sparse Prompting for Adapting MLLMs to Remote Sensing

Qigan Sun, Chaoning Zhang, *Senior Member, IEEE*, Jianwei Zhang, Xudong Wang, Jiehui Xie, Pengcheng Zheng, Haoyu Wang, Sungyoung Lee, *Member, IEEE*, Chi-lok Andy Tai, Yang Yang, *Senior Member, IEEE*, Heng Tao Shen, *Fellow, IEEE*

**Abstract**—In recent years, Multimodal Large Language Models (MLLMs) have made significant progress in visual question answering tasks. However, directly applying existing fine-tuning methods to remote sensing (RS) images often leads to issues such as overfitting on background noise or neglecting target details. This is primarily due to the large-scale variations, sparse target distributions, and complex regional semantic features inherent in RS images. These challenges limit the effectiveness of MLLMs in RS tasks. To address these challenges, we propose a parameter-efficient fine-tuning (PEFT) strategy called Guided Region-Aware Sparse Prompting (GRASP). GRASP introduces spatially structured soft prompts associated with spatial blocks extracted from a frozen visual token grid. Through a question-guided sparse fusion mechanism, GRASP dynamically aggregates task-specific context into a compact global prompt, enabling the model to focus on relevant regions while filtering out background noise. Extensive experiments on multiple RSVQA benchmarks show that GRASP achieves competitive performance compared to existing fine-tuning and prompt-based methods while maintaining high parameter efficiency.

**Index Terms**—Remote sensing, visual question answering, multimodal large language models, soft prompting, parameter-efficient learning.

## I. INTRODUCTION

Remote Sensing Visual Question Answering (RSVQA) is a key task that integrates visual perception with language reasoning, aiming to enable natural language interaction with RS imagery [1], [2]. It provides intuitive and interpretable decision support for object recognition, scene understanding, and spatial relationship analysis, and holds significant value for practical applications such as disaster monitoring, urban planning, and environmental management [3]–[6]. Compared with visual question answering in natural scenes, RSVQA

Qigan Sun, Xudong Wang, and Sungyoung Lee are with the School of Computing, Kyung Hee University, Yongin-si, South Korea (email: sunqian0206@gmail.com; wl200203@khu.ac.kr; sylee@oslab.khu.ac.kr).

Jianwei Zhang, Jiehui Xie, and Pengcheng Zheng are with School of Information and Software Engineering, University of Electronic Science and Technology of China, Chengdu, China (email: zjw5428c@gmail.com; jiehui.xie@std.uestc.edu.cn; zpc777@std.uestc.edu.cn).

Chaoning Zhang and Yang Yang are with the School of Computer Science and Engineering, University of Electronic Science and Technology of China, Chengdu, China (email: chaoningzhang1990@gmail.com; yang.yang@uestc.edu.cn).

Haoyu Wang is with the College of Computer Science and Information Engineering, Harbin Normal University, Harbin, 150025, China (email: w18724284923@outlook.com).

Chi-lok Andy Tai is with College of Professional and Continuing Education, The Hong Kong Polytechnic University, Hong Kong, China (email: andy.tai@cpce-polyu.edu.hk).

Heng Tao Shen is with School of Computer Science and Technology, Tongji University, Shanghai, China (email: shenhengtao@hotmail.com).

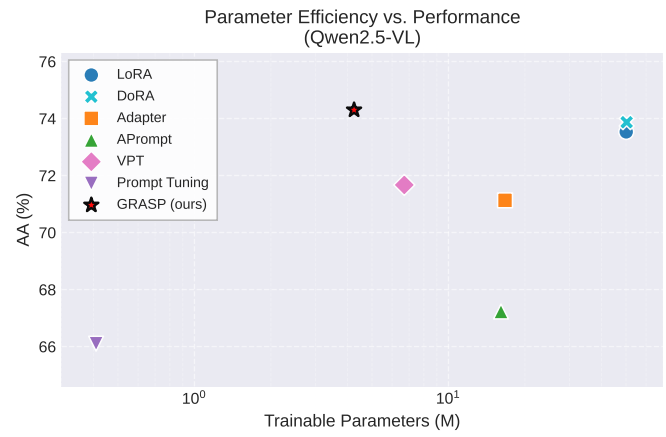


Fig. 1. Parameter efficiency vs. performance on Qwen2.5-VL-7B. The y-axis denotes the overall accuracy (mean of the AA scores on RSVQA-LR, RSVQA-HR, and RSVQA), plotted against trainable parameters (log scale). Our method, GRASP, is represented by a red star. Note that proximity to the top-left corner corresponds to higher accuracy with lower parameter costs.

requires not only the recognition of basic visual elements such as object categories and spatial locations, but also an understanding of spatial context and semantic relationships within the image to perform high-level reasoning over complex questions [7], [8].

Traditional RSVQA methods typically adopt a pipeline consisting of a visual encoder and a task-specific module. For example, early works use convolutional neural networks (e.g., ResNet [9]) to extract image features and combine them with RNNs to process the text [1]. Subsequent works introduce transformers to enhance the fusion and interaction of multimodal features [10], [11]. These features are then passed through a classifier to generate the answers [3]. Although these methods achieve promising performance on specific datasets and task settings, they usually rely on predefined closed-form question sets, and their model architectures and output formats are highly task-dependent [12], [13]. As a result, they lack scalability in open-domain scenarios, limiting their generality and extensibility.

In recent years, Multimodal Large Language Models (MLLMs) have significantly advanced cross-modal semantic alignment and language reasoning capabilities through large-scale multimodal pretraining, enabling a unified framework that supports diverse question formats and natural language-driven interaction [14]. However, directly transferring general-purpose MLLMs to RS visual question answering tasks often

leads to notable performance degradation [15]. One primary reason is that general MLLMs are predominantly pretrained on large-scale natural image–text pairs and therefore lack prior knowledge of ground-object characteristics observed from a top-down perspective [16], [17]. This inherent training data distribution bias makes it difficult for such models to adapt to the substantial domain discrepancies between RS imagery and natural images, including large-scale variations, sparse object distributions, and complex region-level semantic structures. Furthermore, data distribution shifts from different sensors and spatiotemporal conditions further weaken model generalization, exacerbating the difficulty of aligning image content with question semantics [18], [19].

To better adapt general-purpose MLLMs to the RS domain, the prevailing paradigm treats pretrained general MLLMs as backbone models and injects domain-specific knowledge through generic fine-tuning techniques [20]–[22], such as LoRA (Low-Rank Adaptation) [23]. Representative works include GeoChat [24] and EarthGPT [25]. By fine-tuning on large-scale RS multimodal instruction datasets, these studies endow general backbones with preliminary capabilities for RS image understanding and dialogue, thereby validating the feasibility of transferring general large models to RS scenarios [26]. Despite these advances, existing adaptation strategies largely inherit vision–language interaction mechanisms originally designed for natural scenes [27]. We argue that directly applying them to RS tasks has inherent limitations. These methods enforce spatially uniform parameter updates that do not sufficiently account for the distinctive characteristics of RS imagery, namely vast backgrounds with small, sparsely distributed targets. Consequently, such updates often lead to overfitting on dominant background noise while neglecting target details in relevant regions. In this context, Soft Prompting offers a promising avenue via learnable input vectors. We argue that its limited success in RS arises specifically from the lack of spatial customization, not methodological deficiencies. *Overall, existing fine-tuning methods fail to account for the spatial characteristics of RS images, which leads to overfitting on background noise and neglecting target details.*

To this end, we propose Guided Region-Aware Sparse Prompting (GRASP) as a lightweight adaptation strategy for multimodal large models, leveraging soft prompting to provide a more flexible solution by introducing semantic anchors at the input level. Specifically, by associating each spatial block derived from the visual token grid with a learnable soft prompt, our method instantiates these anchors to capture localized semantic cues in a structured and distributed manner. These block-level soft prompts interact with their corresponding visual features conditioned on the input question to estimate task-specific importance, and are subsequently aggregated into a global prompt through a question-guided sparse fusion mechanism. The resulting global prompt is injected as an additional visual token, providing structured visual guidance for the language model without modifying the pretrained vision or language backbones. This design enhances region-aware spatial understanding while maintaining architectural simplicity and strong parameter efficiency. We conduct extensive experiments on multiple RSVQA benchmarks, including ablation studies

on different spatial block configurations. The results show that GRASP achieves competitive performance in answer accuracy and parameter efficiency compared to mainstream fine-tuning and prompt-based approaches, highlighting its effectiveness for RSVQA (see Fig. 1). Our contributions are three-fold:

- We propose Guided Region-Aware Sparse Prompting (GRASP), a PEFT strategy for RS MLLMs that associates learnable soft prompts with spatial blocks to enable region-aware spatial adaptation while keeping the vision and language backbones frozen.
- A question-guided sparse fusion mechanism is introduced to dynamically aggregate spatial context into a compact, task-specific global prompt. This design allows the model to selectively attend to question-relevant regions while effectively filtering out background noise.
- Extensive experiments on multiple RSVQA benchmarks demonstrate that GRASP achieves competitive performance among fine-tuning and prompt-based approaches, while maintaining high parameter efficiency.

## II. RELATED WORK

### A. RS Visual Question Answering

RSVQA lies at the intersection of image understanding, spatial reasoning, and cross-modal semantic modeling. It aims to interpret natural language queries concerning object categories, spatial distributions, and semantic relationships within high-resolution RS imagery [10]. As an important decision-support tool for applications such as disaster monitoring and urban planning, RSVQA poses challenges that are substantially different from those encountered in natural scene VQA. The pronounced scale variation, sparse and uneven object distribution, and complex contextual semantics inherent to RS data significantly hinder effective cross-modal alignment and accurate answer generation [28].

Early studies in RSVQA primarily focus on dataset construction and benchmark establishment, alongside the adaptation of conventional visual question answering architectures. To facilitate supervised learning, datasets such as RSVQA [1] and RSIVQA [29] are constructed through automatic template-based question–answer generation. On the methodological side, initial approaches largely followed the paradigms of generic VQA systems, employing convolutional neural networks for visual feature extraction and recurrent models such as LSTMs for question encoding [30], [31]. To better capture spatial dependencies and relational cues, subsequent works introduce region-level attention mechanisms [32] and Transformer-based cross-modal architectures inspired by advances in vision–language modeling [33]. Despite these improvements, these models represent a closed-set learning paradigm, often lacking the broad commonsense knowledge and robust reasoning capabilities required to fully interpret the intricate semantic relationships in diverse RS scenarios [34].

More recently, research attention has shifted toward adapting MLLMs to the RS domain [35], [36]. By leveraging large-scale vision–language foundation models and fine-tuning them on domain-specific datasets, recent studies report notable gains in cross-modal semantic alignment and reasoning

performance [37], [38]. Nevertheless, the practical deployment of these models is frequently impeded by substantial computational resources and storage overheads. The high cost of extensive model adaptation and prolonged training cycles reduces their flexibility for rapid or resource-constrained applications. As a result, achieving a balance between effective spatial semantic modeling and adaptation efficiency remains an open challenge. In this work, we address this issue by exploring a lightweight, spatially-aware design that captures local semantic information without incurring the overhead of full-parameter adaptation.

### B. Fine-tuning Strategies for MLLMs

With the rapid development of multimodal learning, researchers have focused on fine-tuning large-scale multimodal models to integrate heterogeneous data such as images and text, thereby improving their performance on specific tasks [39], [40]. Based on the parameter update strategy and mechanism, existing fine-tuning methods can be broadly categorized into full fine-tuning, PEFT based on adapters, and prompt tuning.

**Full Fine-tuning.** Traditional full fine-tuning typically follows a transfer learning framework, where all parameters are updated based on a pretrained model. By jointly optimizing the network parameters of different modalities, this approach enhances semantic alignment. Early Vision-Language models and the instruction-tuning stage of some MLLMs (e.g., LLaVA) employ this strategy to achieve strong reasoning capabilities [41], [42]. However, as model size grows exponentially, full fine-tuning incurs prohibitive computational and storage costs and is prone to catastrophic forgetting, limiting its practicality for rapid domain adaptation.

**Parameter-Efficient Fine-tuning.** To alleviate computational resource constraints, researchers have proposed PEFT methods that freeze the pretrained backbone and update only a small subset of parameters. Representative approaches include Adapters, which insert lightweight bottleneck networks between layers [43], and LoRA, which approximates weight updates via low-rank matrix factorization. As a non-intrusive alternative to these architectural modifications, Prompt Tuning adapts models by optimizing learnable context representations in the input space [44]. This paradigm has been successfully adapted to vision-language models (e.g., CoOp [45], [46]) and visual encoders (VPT [47]), with deep variants injecting prompts into intermediate layers [48]. In the RS domain, methods like C-SAW [49] and MVP [50] leverage prompts to mitigate domain shift. However, these approaches typically rely on static, image-level prompts designed for classification, lacking the dynamic, question-guided mechanisms necessary for modeling region-level spatial relationships. To address this gap, we propose GRASP, a lightweight, spatially-aware strategy tailored for RSVQA.

### III. METHODOLOGY

GRASP partitions the visual token grid into spatial blocks and associates each block with a learnable soft prompt. It then computes question-conditioned sparse weights to aggregate

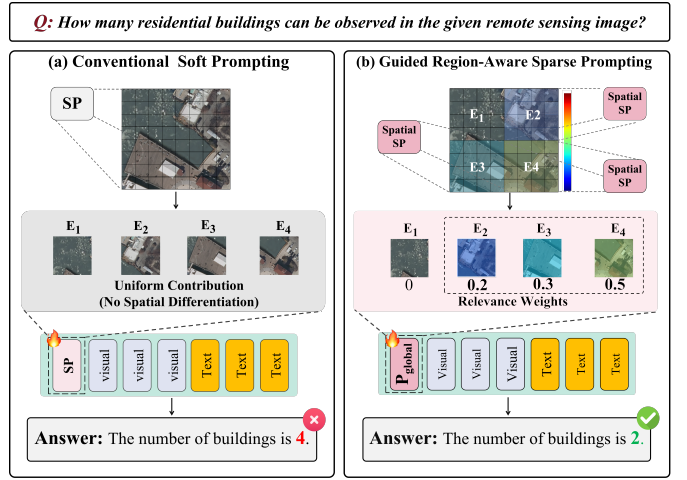


Fig. 2. Conceptual comparison between Conventional soft prompting and GRASP. (a) Conventional soft prompting: Relies on static, uniform prompts. It struggles to suppress background interference (e.g.,  $E_1$ ), as it lacks region-aware adaptation. (b) GRASP: Utilizes question-guided sparse weighting to suppress irrelevant backgrounds ( $E_1$  weight=0) and emphasize targets ( $E_4$  weight=0.5). The resulting global prompt  $P_{global}$  is computed by weighted fusion over all regions, where regions with zero weights are ignored.

block-wise prompts into a single global prompt, which is injected as an additional visual token to guide answer generation by a frozen language model. During training, supervision signals backpropagate only to the soft prompts and lightweight projection layers, while the vision and language backbones remain fixed, with the concept diagram comparing traditional SP and our approach shown in Fig. 2. To clearly describe the workflow, we decompose GRASP into four components: (A) Spatial Block-based Feature Encoding with Soft Prompts, (B) Question-guided Sparse Soft Prompt Fusion, (C) Optimization Objective and Training Strategy, and (D) Parameter and Computational Complexity. Fig. 3 provides an overview of the GRASP framework.

#### A. Spatial Block-based Feature Encoding with Soft Prompts

RS images usually exhibit high spatial resolution and complex structural layouts. To capture region-specific local semantics while remaining compatible with large-scale vision-language models, we construct spatial block-level visual representations based on the visual token grid produced by a frozen vision encoder, and introduce corresponding block-wise soft prompts to bridge spatial visual information and language reasoning. Given an input image  $x \in \mathbb{R}^{H \times W \times 3}$ , where  $H$  and  $W$  denote the image height and width, the frozen visual backbone encodes the image into  $M = H_t \times W_t$  visual tokens  $\mathcal{T} = \{t_1, \dots, t_M\}$ . Each token  $t_j \in \mathbb{R}^{d_v}$  represents a  $d_v$ -dimensional visual feature vector, and all tokens are arranged in a two-dimensional grid of size  $H_t \times W_t$ , preserving the spatial layout of the original image. We uniformly partition the visual token grid into  $N$  non-overlapping spatial blocks  $\mathcal{B} = \{B_1, \dots, B_N\}$ , where each block  $B_i \subset \mathcal{T}$  contains a set of spatially adjacent visual tokens. Let  $|B_i|$  denote the number of tokens in the  $i$ -th block. We obtain the block-level visual

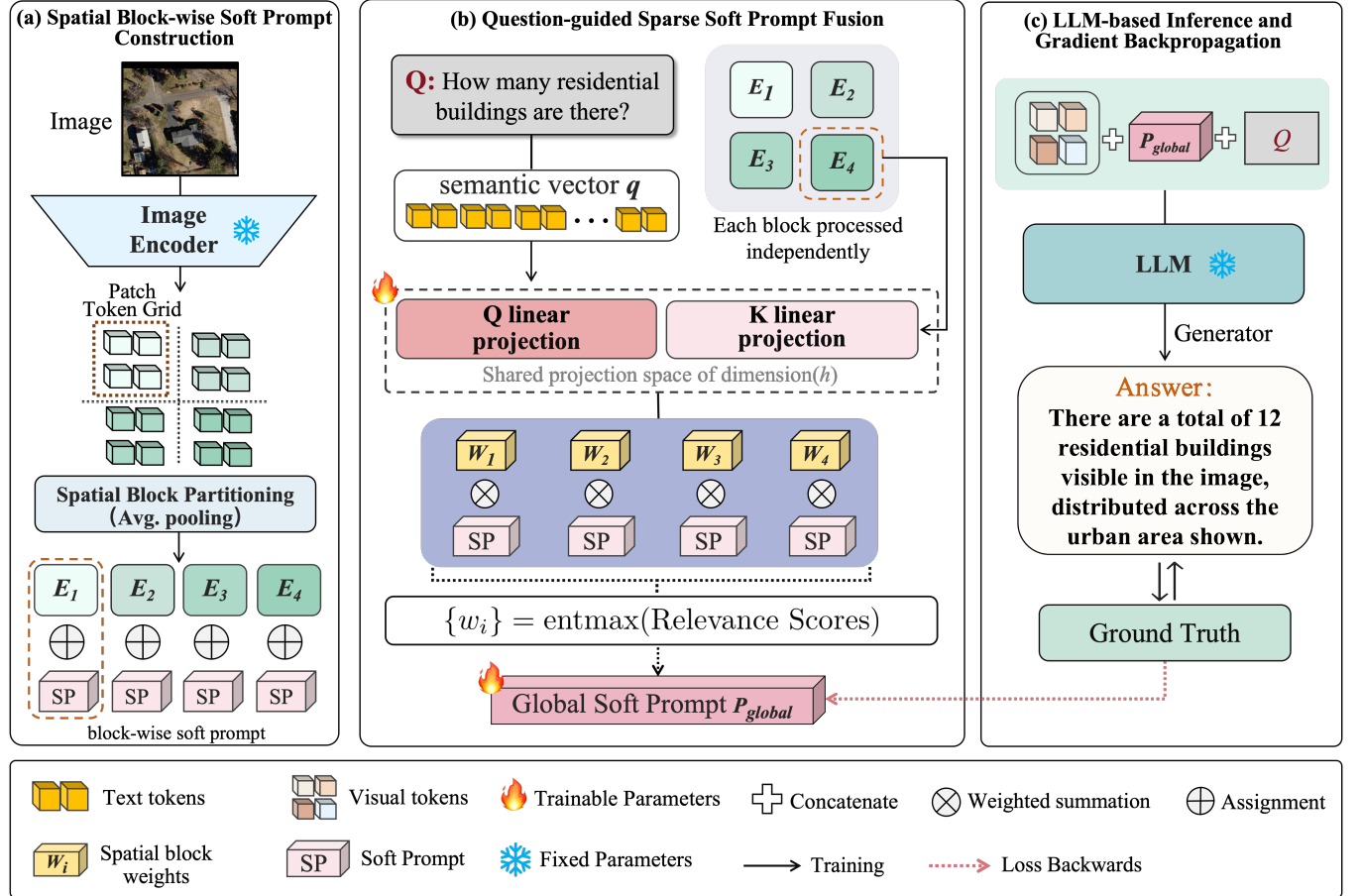


Fig. 3. Architecture of the GRASP framework. (a) **Spatial Block-wise Soft Prompt Construction**: The frozen vision encoder generates a visual token grid from the image. Average pooling partitions this grid into spatial blocks (e.g.,  $E_1$ – $E_4$ ), where each block  $E_i$  links to a learnable local soft prompt (SP). (b) **Question-guided Sparse Soft Prompt Fusion**: The frozen LLM derives a semantic vector  $q$  from the question. The system projects  $q$  and block-level features  $E_i$  into a shared space to compute relevance scores. Entmax activation converts these scores into sparse weights  $\{w_i\}$ , which the model uses to aggregate local SPs into a task-specific global soft prompt  $P_{global}$ . (c) **LLM-based Inference and Gradient Backpropagation**: The framework injects  $P_{global}$  into the multimodal token sequence to guide the frozen LLM in answer generation. Training updates only the soft prompts and linear projection parameters.

representation by average pooling the tokens within the block and adding a fixed positional encoding:

$$E_i = \frac{1}{|B_i|} \sum_{t_j \in B_i} t_j + PE_i, \quad (1)$$

where  $E_i \in \mathbb{R}^{d_v}$  denotes the visual feature of the  $i$ -th spatial block, and  $PE_i \in \mathbb{R}^{d_v}$  is a fixed positional encoding that represents the relative spatial location of the block. Specifically, given  $N$  spatial blocks, we introduce a set of block-wise soft prompts  $\{p_1, \dots, p_N\}$ , where each  $p_i \in \mathbb{R}^{d_p}$  is a  $d_p$ -dimensional trainable parameter initialized from a zero-mean Gaussian distribution,  $p_i \sim \mathcal{N}(0, \sigma^2 I)$ , with  $\sigma^2$  denoting the initialization variance. These soft prompts do not encode visual content directly. Instead, they serve as task-level semantic adapters that model how information from different spatial regions should influence the language model during multimodal reasoning. By assigning distinct soft prompts to different spatial blocks, the model explicitly captures structural differences among regions within an image without modifying the frozen visual backbone.

### B. Question-guided Sparse Soft Prompt Fusion

To selectively integrate block-level semantic cues, we propose a Question-guided Sparse Fusion mechanism. This process can be viewed as a query-guided attention operation with a decoupled Key–Value formulation, where visual spatial features determine where to attend, while learnable soft prompts specify what information to inject. Given an input question, we extract a pooled textual representation  $q \in \mathbb{R}^{d_t}$  by forwarding the question tokens through the frozen language model and mean-pooling the hidden states. To compute relevance in a shared latent space, both the question representation and block-level visual features are projected into a low-dimensional attention space of dimension  $h$ :

$$k_i = \text{Proj}_K^{(v)}(E_i), \quad \tilde{q} = \text{Proj}_Q^{(t)}(q), \quad (2)$$

where  $\text{Proj}_K^{(v)} : \mathbb{R}^{d_v} \rightarrow \mathbb{R}^h$  and  $\text{Proj}_Q^{(t)} : \mathbb{R}^{d_t} \rightarrow \mathbb{R}^h$  are learnable linear projections for visual and textual features, respectively. We then measure the relevance of each spatial block via scaled dot-product similarity:

$$s_i = \frac{k_i^\top \tilde{q}}{\sqrt{h}}, \quad i = 1, \dots, N. \quad (3)$$

Here,  $s_i$  measures the relevance between the question and the  $i$ -th spatial block. The factor  $\sqrt{h}$  scales the dot-product scores to stabilize their magnitude. To encourage sparsity and suppress irrelevant regions, the relevance scores are normalized using the Entmax [51] function:

$$\mathbf{w} = \text{entmax}_\alpha(\mathbf{s}). \quad (4)$$

Here,  $\mathbf{w} = [w_1, \dots, w_N]^\top$  denotes the sparse importance weights. The hyperparameter  $\alpha$  governs the sparsity level of Entmax, with  $\alpha = 1$  reducing to Softmax and larger values producing sparser weights. Finally, the block-wise soft prompts are aggregated into a single global prompt through a question-conditioned sparse weighting scheme:

$$p_{\text{global}} = \sum_{i=1}^N \left[ \text{entmax}_\alpha \left( \frac{\{\text{Proj}_K^{(v)}(E_j)^\top \text{Proj}_Q^{(t)}(q)\}_{j=1}^N}{\sqrt{h}} \right) \right] \cdot p_i. \quad (5)$$

In this unified formulation,  $E_j$  refers to the spatial block representations defined in Eq. (1), while  $p_{\text{global}} \in \mathbb{R}^{d_p}$  constitutes a task-specific parametric instruction summarizing question-relevant spatial regions (with  $d_p = d_v$  to enable concatenation with visual tokens). We inject the derived  $p_{\text{global}}$  at the vision-language interface by constructing an extended visual input sequence as follows:

$$\mathcal{T}' = [p_{\text{global}}, \mathcal{T}]. \quad (6)$$

The operator  $[\cdot, \cdot]$  signifies concatenation along the sequence length dimension. The resulting spatially-enhanced sequence  $\mathcal{T}'$  is then fed into the multimodal model, where it modulates the reasoning process.

### C. Optimization Objective and Training Strategy

The language model performs autoregressive answer generation conditioned on the spatially-enhanced multimodal representation. Specifically, we concatenate the extended visual sequence  $\mathcal{T}'$  (derived in Eq. (6)) with the tokenized question embeddings  $X_Q$  to form the input context:

$$\mathcal{X}_{\text{in}} = [\mathcal{T}', X_Q]. \quad (7)$$

This combined sequence is fed into a frozen pretrained language decoder, which computes the conditional probability of the target answer  $Y = \{y_1, \dots, y_L\}$ . The optimization objective is to minimize the negative log-likelihood of the ground-truth tokens:

$$\mathcal{L}(\Theta) = - \sum_{t=1}^L \log P_{\text{LM}}(y_t \mid y_{<t}, \mathcal{X}_{\text{in}}; \Theta), \quad (8)$$

where  $y_{<t}$  denotes the preceding generated tokens. Crucially, during backpropagation, gradients are computed solely with respect to the trainable parameter set  $\Theta = \{\{p_i\}_{i=1}^N, \text{Proj}_K^{(v)}, \text{Proj}_Q^{(t)}\}$ . The massive parameters of the visual encoder and the language model remain frozen. This selective optimization ensures the model adapts to the RS domain through the lightweight soft prompts and fusion layers, maintaining parameter efficiency while preserving the generalization capability of the pretrained backbone.

### D. Parameter and Computational Complexity Analysis

Following the training setup described above, we analyze the parameter and computational complexity of GRASP. Recall that the trainable parameter set is defined as  $\Theta = \{\{p_i\}_{i=1}^N, \text{Proj}_K^{(v)}, \text{Proj}_Q^{(t)}\}$ . In the parameter analysis, we denote the learnable weight matrices corresponding to the projection layers as  $\mathbf{W}_K \in \mathbb{R}^{h \times d_v}$  and  $\mathbf{W}_Q \in \mathbb{R}^{h \times d_t}$ , respectively. To align multimodal semantics, GRASP projects the textual intent  $q$  and block-level visual features  $E_i$  into a shared low-rank latent space  $\mathbb{R}^h$ . Consequently, the total learnable parameter count,  $|\Theta_{\text{train}}|$ , decomposes into:

$$\begin{aligned} |\Theta_{\text{train}}| &= \text{Params}(\{p_i\}_{i=1}^N) + \text{Params}(\text{Proj}_K^{(v)}) + \text{Params}(\text{Proj}_Q^{(t)}) \\ &= \underbrace{N \times d_p}_{\text{Soft Prompts}} + \underbrace{(h \times d_v + h \times d_t)}_{\text{Projection Matrices}} \\ &= \mathcal{O}(Nd_p + h(d_v + d_t)). \end{aligned} \quad (9)$$

Although the parameter count is primarily governed by the projection dimension  $h$ , the total size (typically  $\approx 4\text{M}$ ) remains negligible compared to the billions of parameters in the frozen backbone. This formulation significantly reduces the optimization search space and storage overhead. Regarding computational complexity, our method offers a dual advantage. First, the per-sample complexity of the fusion module  $T_{\text{fusion}}$  is linear with respect to the number of blocks  $N$ :

$$\begin{aligned} T_{\text{fusion}} &= T_{\text{proj}}(q) + \sum_{i=1}^N T_{\text{proj}}(E_i) + T_{\text{agg}}(p_{\text{global}}) \\ &= \mathcal{O}(N(d_v h + d_p)). \end{aligned} \quad (10)$$

Since  $\mathcal{O}(T_{\text{fusion}})$  is several orders of magnitude smaller than the Transformer layers, the module introduces negligible latency. More importantly, GRASP introduces a highly efficient modulation mechanism for MLLM inference. Instead of injecting a large number of task-specific tokens or modifying the original visual representations, our fusion strategy produces a single global soft prompt token that summarizes question-relevant spatial regions, while retaining the original visual token sequence unchanged. This design introduces only a one-token overhead to the multimodal input, thereby preserving the inference efficiency of the pretrained language model while enabling spatially aware reasoning.

## IV. EXPERIMENTS

### A. Dataset Descriptions

To evaluate the effectiveness of our proposed GRASP method in RSVQA tasks, we use two widely adopted datasets: RSVQA [1] and RSIVQA [29]. The RSVQA dataset consists of two subsets: a low-resolution subset (Sentinel-2, 10m resolution,  $256 \times 256$  pixels) and a high-resolution subset (USGS HRO, 15cm resolution,  $512 \times 512$  pixels). The low-resolution subset contains 772 images with 77,232 IQA triplets, while the high-resolution subset includes 10,659 images and 1,066,316 IQA triplets. Questions in the dataset fall into four categories: Count, Presence, Comparison, and Rural/Urban, with the high-resolution subset also including the Area category.

TABLE I

UNIFIED RESULTS OF LLAVA-NEXT ON THREE BENCHMARKS. PARAMS (M) DENOTES TRAINABLE PARAMETERS (MILLIONS). COUNT, R/U, PRES., AND COMP. CORRESPOND TO DIFFERENT QUESTION CATEGORIES, NAMELY COUNTING, RURAL/URBAN, PRESENCE, AND COMPARISON. AA DENOTES AVERAGE ACCURACY. **GREEN** VALUES INDICATE GAINS OVER THE BASE MODEL. **BOLD** AND UNDERLINE MARK THE BEST AND SECOND-BEST RESULTS.

Method	Params	RSVQA-LR					RSVQA-HR					RSIVQA				
		Count	R/U	Pres.	Comp.	AA	Count	Area	Pres.	Comp.	AA	Yes/No	Num.	Other	AA	
LLaVA-Next (Base)	-	23.8	71.0	55.4	66.5	54.2	56.0	49.1	66.4	75.6	61.8	85.5	45.1	40.2	56.9	
<b>Additive parameter tuning methods</b>																
+ Adapter	16.7	28.0 (+4.2)	81.9 (+10.9)	74.6 (+19.2)	77.1 (+10.6)	65.4 (+11.2)	63.1	<u>68.8</u>	78.4	80.9	72.8	90.3	60.7 (+15.6)	76.3 (+36.1)	75.8 (+18.9)	
+ LoRA	50.1	29.5 (+5.7)	84.0 (+13.0)	77.3 (+21.9)	<b>79.0</b> (+12.5)	67.5 (+13.3)	64.2	68.6	78.6	81.8	73.3	<u>91.2</u>	62.0 (+16.9)	78.4 (+38.2)	77.2 (+20.3)	
+ DoRA	50.2	30.1 (+6.3)	<u>84.3</u> (+13.3)	<u>77.4</u> (+22.0)	78.7 (+12.2)	<u>67.6</u> (+13.4)	<u>64.8</u> (+8.8)	68.5	<u>79.0</u> (+19.4)	<u>82.1</u> (+12.6)	73.6	<u>91.2</u> (+6.5)	62.7 (+11.8)	<u>78.7</u> (+5.7)	<u>77.5</u> (+38.5)	77.5 (+20.6)
<b>Prompt-based tuning methods</b>																
+ Prompt Tuning	0.41	24.1 (+0.3)	78.3 (+7.3)	68.5 (+13.1)	70.3 (+3.8)	60.3 (+6.1)	57.4	53.9	70.2	76.7	64.6	88.1	51.5 (+6.4)	68.7 (+28.5)	69.4 (+12.5)	
+ APrompt	16.1	26.8 (+3.0)	79.8 (+8.8)	69.0 (+13.6)	72.2 (+5.7)	62.0 (+6.8)	58.6	57.4	71.9	77.2	66.3	89.0	53.0 (+3.5)	70.8 (+7.9)	70.9 (+30.6)	70.9 (+14.0)
+ VPT	6.70	31.9 (+8.1)	80.4 (+9.4)	75.5 (+20.1)	76.9 (+10.4)	66.2 (+12.0)	61.5	67.3	78.5	80.1	71.9	90.8	<u>62.9</u> (+5.3)	75.4 (+17.8)	76.4 (+35.2)	76.4 (+19.5)
+ GRASP (ours)	<b>4.25</b>	<b>32.8</b> (+9.0)	<b>85.7</b> (+14.7)	<b>77.5</b> (+22.1)	<b>78.8</b> (+12.3)	<b>68.7</b> (+14.5)	<b>65.3</b> (+9.3)	<b>69.5</b> (+20.4)	<b>79.2</b> (+12.8)	<b>82.3</b> (+6.7)	<b>74.1</b> (+12.3)	<b>92.4</b> (+6.9)	<b>63.6</b> (+18.5)	<b>78.9</b> (+38.7)	<b>78.3</b> (+21.4)	

The RSIVQA dataset contains 37,264 images and 111,693 IQA triplets, collected from various RS scene datasets such as UCM, Sydney, AID, HRRSD, and DOTA. The questions are categorized into three types: Yes/No, Number, and Others (e.g., spatial relation questions). Both datasets combine automated generation and manual annotation, providing a solid foundation for evaluating our method’s capabilities in global prompt structuring and local semantic modeling. To ensure a fair comparison of model performance, we adopt the same dataset split as in [29], using stratified sampling to allocate 80% of the dataset to the training set, 10% to the validation set, and the remaining 10% to the test set.

### B. Experimental Details

All experiments are conducted on a single NVIDIA RTX 3090 GPU. We employ the AdamW optimizer with an initial learning rate of  $1 \times 10^{-4}$  and weight decay of 0.01. The learning rate is warmed up linearly over the first 10% of total training steps, followed by linear decay. Training uses a batch size of 6 for up to 20 epochs, with early stopping triggered by validation accuracy (patience of 5).

Our evaluation focuses on two representative 7B-scale vision-language models: LLava-Next-7B [52] and Qwen2.5-VL-7B [53]. To ensure a fair comparison, we adhere strictly to their official preprocessing pipelines and keep the vision encoders frozen during fine-tuning.

Regarding image preprocessing, we preserve the native  $512 \times 512$  resolution of RSVQA-HR images to retain their high-resolution details. For RSVQA-LR and RSIVQA, which have varying or lower native resolutions, we resize the images to  $224 \times 224$ . This unification facilitates consistent spatial block partitioning in our GRASP module and enables stable control over the block count  $N$  across datasets.

The proposed GRASP uses a bottleneck dimension  $h = 512$ , with the soft prompt dimension aligned to the lan-

guage model’s hidden size and an Entmax sparsity parameter  $\alpha = 1.5$ . The spatial block count  $N$  is treated as a key hyperparameter and selected through ablation studies (see Section IV-E). In the main experiments, we set  $N = 4$  for RSVQA-LR and RSIVQA, and  $N = 16$  for RSVQA-HR.

Following the standard evaluation protocol of RSVQA [1], we report the Accuracy metric based on exact matching between the predicted answer and the ground truth. To bridge the gap between free-form text generation in MLLMs and the fixed-vocabulary answer space of the datasets, we apply standard text normalization to model outputs (lowercasing, punctuation removal, and converting number words to digits) before computing accuracy.

For a fair comparison, all baseline methods keep the vision encoder frozen. VPT [47] introduces learnable visual prompt tokens into the visual Transformer while maintaining fixed backbone weights. Adapter [43] (hidden dimension = 64) is applied to the Transformer layers of the language model. LoRA [23] (rank = 64) and DoRA [54] (rank = 64) are both applied to the same set of linear projections in the language model Transformer for a controlled comparison. Prompt Tuning [44] and APrompt [48] inject prompt tokens at the input or intermediate layers. This setting allows performance differences to primarily reflect the effectiveness of different adaptation strategies.

### C. Performance Evaluation

In this section, we evaluate GRASP against existing fine-tuning paradigms and examine the trade-off between reasoning accuracy and parameter efficiency across two representative MLLM backbones, namely LLava-Next and Qwen2.5-VL. As shown in Tables I and II, GRASP demonstrates competitive performance on all benchmarks while maintaining a relatively small parameter footprint. Taking Qwen2.5-VL as a representative example, GRASP achieves 72.5% average accuracy

TABLE II

UNIFIED RESULTS OF QWEN2.5-VL-7B ON THREE BENCHMARKS. PARAMS (M) DENOTES TRAINABLE PARAMETERS (MILLIONS). THE ABBREVIATIONS FOLLOW THE SAME DEFINITIONS AS IN TABLE I. **GREEN** VALUES INDICATE GAINS OVER THE BASE MODEL. **BOLD** AND UNDERLINE MARK THE BEST AND SECOND-BEST RESULTS.

Method	Params	RSVQA-LR					RSVQA-HR					RSIVQA			
		Count	R/U	Pres.	Comp.	AA	Count	Area	Pres.	Comp.	AA	Yes/No	Num.	Other	AA
Qwen2.5-VL (Base)	–	20.9	66.0	62.3	71.4	55.2	52.6	61.4	65.6	76.4	64.0	87.3	43.8	38.7	56.6
<b>Additive parameter tuning methods</b>															
+ Adapter	16.7	27.6 (+6.7)	81.4 (+15.4)	79.0 (+16.7)	80.5 (+9.1)	67.1 (+11.9)	60.3	69.7	66.4	80.3	69.2	90.5 (+3.2)	58.0 (+14.2)	82.8 (+44.1)	77.1 (+20.5)
+ LoRA	50.1	29.5 (+8.6)	<b>83.0</b> (+17.0)	80.8 (+18.5)	<u>81.3</u> (+9.9)	68.7 (+13.5)	62.1	70.6	70.3	81.9	71.2	<b>92.0</b> (+4.7)	60.9 (+17.1)	<b>89.2</b> (+50.5)	80.7 (+24.1)
+ DoRA	50.2	30.0 (+9.1)	<u>82.9</u> (+16.9)	<u>81.2</u> (+18.9)	81.1 (+9.7)	<u>68.8</u> (+13.6)	<u>62.4</u> (+9.8)	<u>70.8</u> (+9.4)	<u>71.0</u> (+5.4)	<u>82.1</u> (+5.7)	71.6 (+7.6)	91.7 (+4.4)	61.1 (+17.3)	<u>89.0</u> (+50.3)	80.6 (+24.0)
<b>Prompt-based tuning methods</b>															
+ Prompt Tuning	0.41	22.3 (+1.4)	77.8 (+11.8)	71.4 (+9.1)	72.9 (+1.5)	61.1 (+5.9)	54.1	63.0	67.1	78.5	65.7	89.3 (+2.0)	50.2 (+6.4)	75.1 (+36.4)	71.5 (+14.9)
+ APrompt	16.1	23.4 (+2.5)	78.1 (+12.1)	72.5 (+10.2)	73.0 (+1.6)	61.8 (+6.6)	56.3	64.2	67.4	79.4	66.8	90.4 (+3.1)	51.6 (+7.8)	77.4 (+38.7)	73.1 (+16.5)
+ VPT	6.70	<u>30.3</u> (+9.4)	80.9 (+14.9)	79.3 (+17.0)	79.3 (+7.9)	67.5 (+12.3)	61.2	68.4	68.2	80.5	69.6	91.2 (+3.9)	<u>61.2</u> (+17.4)	81.4 (+42.7)	77.9 (+21.3)
+ GRASP (ours)	<b>4.25</b>	<b>31.1</b> (+10.2)	82.6 (+16.6)	<b>81.6</b> (+19.3)	<b>81.5</b> (+10.1)	<b>69.2</b> (+14.0)	<b>62.7</b> (+10.1)	<b>71.0</b> (+9.6)	<b>73.9</b> (+8.3)	<b>82.5</b> (+6.1)	<b>72.5</b> (+8.5)	<b>93.1</b> (+5.8)	<b>61.5</b> (+17.7)	<b>89.0</b> (+50.3)	<b>81.2</b> (+24.6)

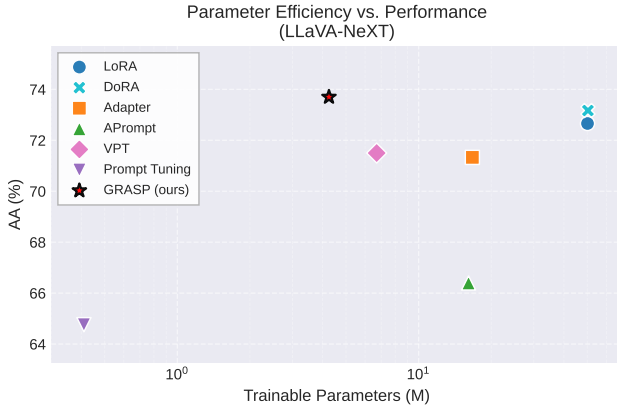


Fig. 4. Parameter efficiency vs. performance on LLaVA-Next. The y-axis denotes the overall accuracy (mean of the AA scores on RSVQA-LR, RSVQA-HR, and RSIVQA), plotted against trainable parameters (log scale). Our method, GRASP, is represented by a red star. Note that proximity to the top-left corner corresponds to higher accuracy with lower parameter costs.

(AA) on RSVQA-HR, yielding a modest gain over LoRA (71.2%) and slightly higher AA than its enhanced variant DoRA (71.6%). Importantly, GRASP attains this improvement with substantially lower computational overhead: while LoRA updates 50.1M parameters (0.72% of the backbone), GRASP requires only 4.25M trainable parameters (0.06%), corresponding to an 11.8 $\times$  reduction in trainable weights. This consistent performance gap across both backbones suggests a key difference in adaptation mechanisms. While LoRA applies low-rank updates globally to model weights, GRASP employs a spatially explicit prompting strategy that associates learnable soft prompts with specific image regions. This region-aware design better preserves localized semantic information, enabling more effective capture of spatial nuances in RS imagery.

Furthermore, compared with VPT, a representative prompt-based method, GRASP improves accuracy by 2.9% on

RSVQA-HR and 1.7% on RSVQA-LR when using the Qwen2.5-VL backbone. These gains support the hypothesis that the global prompts used in standard prompt tuning are insufficient for spatially dispersed targets in RS imagery. By decomposing visual cues into region-aware sparse prompts and aggregating them through a question-guided fusion mechanism, GRASP effectively filters irrelevant background information and enhances region-specific spatial semantic modeling. This advantage is further illustrated in Fig. 1 and 4, which visualizes the trade-off between parameter efficiency and performance. In the scatter plot, GRASP (marked with a red star) occupies the upper-left region, indicating a favorable balance between accuracy and parameter cost. Overall, these results suggest that structural alignment with visual content, rather than merely increasing parameter scale, plays a more decisive role in effective adaptation for RS tasks.

#### D. Qualitative Results

To provide intuitive insights into how GRASP performs cross-modal reasoning, we visualize representative success cases and their corresponding attention heatmaps in Fig. 5. These heatmaps are obtained by projecting the learned question-guided sparse fusion weights onto the original image spatial blocks, illustrating how the model allocates spatial attention under different queries. As shown in the high-resolution examples, GRASP exhibits clear question-dependent spatial activation patterns. For instance, when answering whether a commercial building is present (Q1), the model assigns higher weights to spatial blocks covering large flat-roofed structures, while assigning lower weights to surrounding regions. In object counting queries (Q2), the activated blocks correspond to multiple distinct building instances, indicating that the model attends to individual objects relevant to the counting task. Similarly, for road-related questions (Q3), GRASP emphasizes elongated linear regions that align

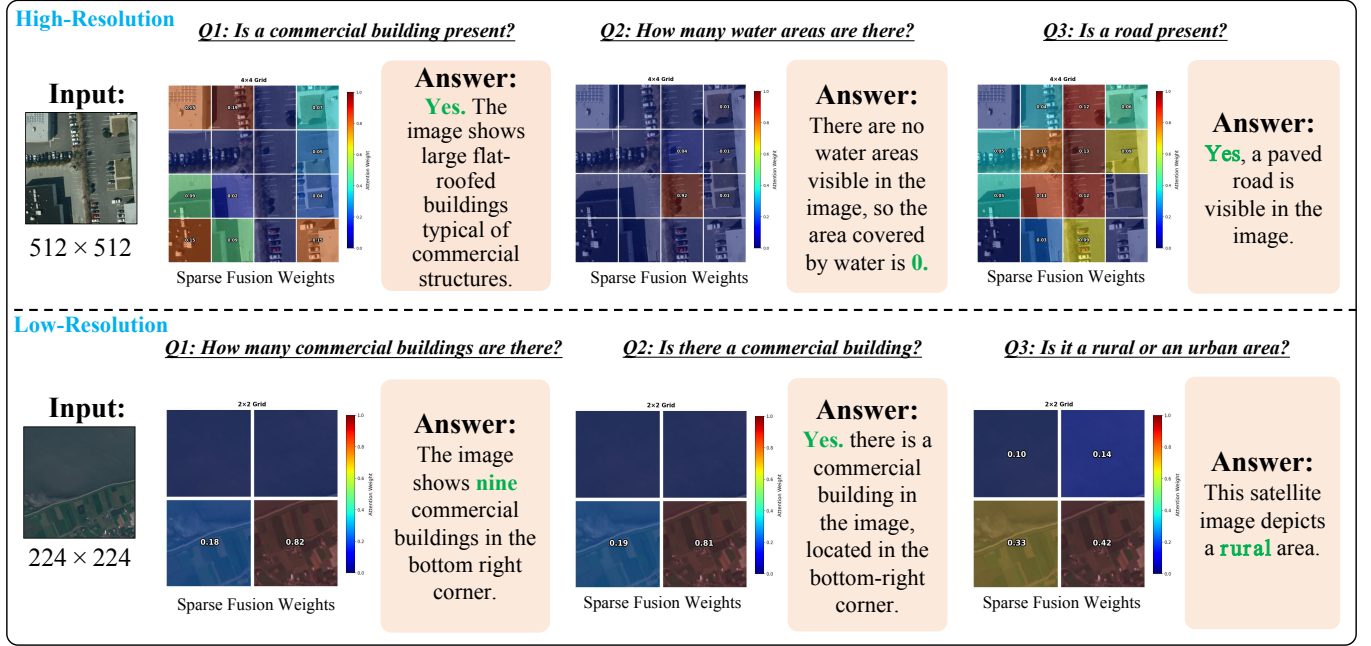


Fig. 5. **Visualization of Question-guided Sparse Fusion Weights across different input resolutions.** The top row shows the  $4 \times 4$  grid weights for the  $512 \times 512$  input, while the bottom row displays the  $2 \times 2$  grid for the  $224 \times 224$  input. These weights represent the contribution of each spatial block to the final representation, with answers highlighted in green denoting correct predictions.

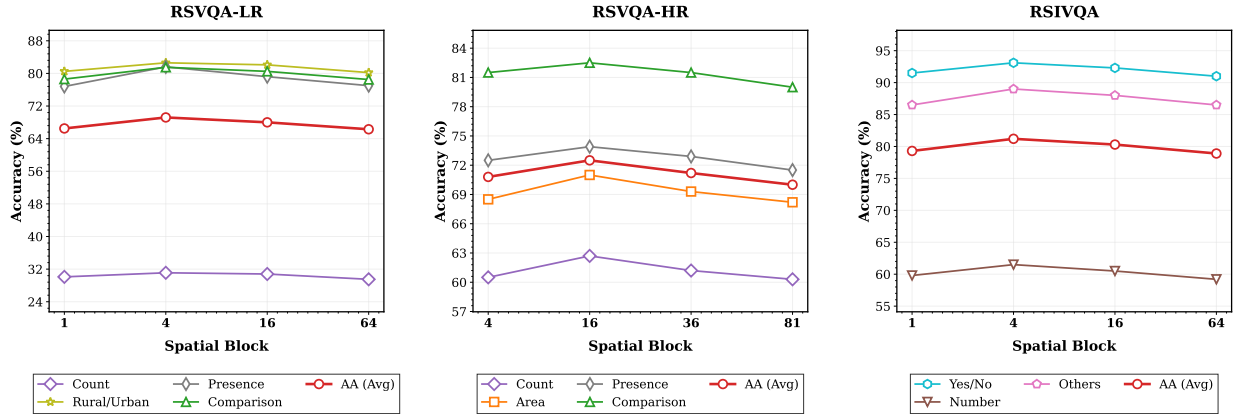


Fig. 6. Impact of spatial block count ( $N$ ) on performance with the Qwen2.5-VL-7B backbone across RSVQA-LR, RSVQA-HR, and RSIVQA datasets.

with paved road structures in the image. A similar behavior can be observed under low-resolution inputs, where GRASP selectively focuses on a small subset of spatial blocks associated with the queried semantic concepts. Despite reduced visual detail, the sparse fusion weights remain concentrated on regions that are most informative for the given question, suggesting that the spatially explicit prompting mechanism facilitates localized visual reasoning across different input resolutions.

#### E. Ablation Study

In this section, we conduct a comprehensive ablation study to evaluate the impact of key architectural hyperparameters on the performance of GRASP. Specifically, we focus on two critical factors governing the model's spatial reasoning capability: the granularity of spatial block partitioning ( $N$ ) and the

sparsity level of the Entmax-based prompt fusion mechanism ( $\alpha$ ). To maintain conciseness while ensuring representative analysis, we report all ablation results using the Qwen2.5-VL-7B backbone.

**Number of Spatial Blocks.** We investigate the impact of the spatial block count  $N$  on model performance, as the granularity of spatial partitioning directly determines the trade-off between local semantic detail and feature integrity. As Fig. 6 illustrates, the optimal number of blocks varies depending on the inherent resolution of the dataset. For the RSVQA-LR and RSIVQA datasets, which generally contain lower-resolution imagery or larger distinct objects, performance peaks at  $N = 4$  (a  $2 \times 2$  grid). Increasing the block count further to 16 or 64 causes a noticeable decline in accuracy. This indicates that for lower-resolution inputs, excessive partitioning fragments the visual features into meaningless patches, which disrupts

TABLE III

UNIFIED ABLATION ON ENTMAX SPARSITY PARAMETER  $\alpha$  FOR GRASP ON QWEN2.5-VL-7B ACROSS RSVQA-LR, RSVQA-HR, AND RSIVQA DATASETS.  $\alpha = 1.0$  AND  $\alpha = 2.0$  CORRESPOND TO SOFTMAX AND SPARSEMAX, RESPECTIVELY. RESULTS ARE REPORTED AS ACCURACY (%). THE BLOCK NUMBER  $N$  IS FIXED TO THE BEST SETTING FROM THE BLOCK-NUMBER ABLATION (RSVQA-LR/RSIVQA:  $N = 4$ ; RSVQA-HR:  $N = 16$ ).

$\alpha$	RSVQA-LR					RSVQA-HR					RSIVQA			
	Count	R/U	Pres.	Comp.	AA	Count	Area	Pres.	Comp.	AA	Yes/No	Num.	Other	AA
1.0	28.4	79.2	78.0	78.1	65.9	59.5	68.0	70.5	78.8	69.2	91.0	58.7	82.6	77.4
1.2	29.6	81.0	79.7	79.9	67.6	61.1	69.4	72.0	80.5	70.8	91.8	60.0	86.2	79.3
<b>1.5</b>	<b>31.1</b>	<b>82.6</b>	<b>81.6</b>	<b>81.5</b>	<b>69.2</b>	<b>62.7</b>	<b>71.0</b>	<b>73.9</b>	<b>82.5</b>	<b>72.5</b>	<b>93.1</b>	<b>61.5</b>	<b>89.0</b>	<b>81.2</b>
1.8	30.5	81.5	80.5	80.6	68.3	61.8	70.1	72.5	81.2	71.4	92.6	60.7	88.1	80.5
2.0	29.3	80.1	78.9	79.3	66.9	60.5	68.7	71.4	79.9	70.1	92.2	60.3	86.8	79.8

TABLE IV

ABLATION RESULTS COMPARING ORIGINAL GRASP (BASELINE) AND THE UNIFORM SOFT PROMPT VARIANT (WITHOUT QUESTION GUIDANCE) ON QWEN2.5-VL-7B. **RED** VALUES INDICATE PERFORMANCE DROPS RELATIVE TO GRASP. **BOLD** MARKS THE BEST RESULTS.

Metric	GRASP (Baseline)	Uniform Prompts
	RSVQA-LR	
<b>RSVQA-LR</b>		
Count	<b>31.1</b>	26.4 ( <b>-4.7</b> )
R/U	<b>82.6</b>	78.3 ( <b>-4.3</b> )
Pres.	<b>81.6</b>	79.0 ( <b>-2.6</b> )
Comp.	<b>81.5</b>	77.9 ( <b>-3.6</b> )
AA	<b>69.2</b>	65.4 ( <b>-3.8</b> )
<b>RSVQA-HR</b>		
Count	<b>62.7</b>	58.6 ( <b>-4.1</b> )
Area	<b>71.0</b>	67.6 ( <b>-3.4</b> )
Pres.	<b>73.9</b>	71.7 ( <b>-2.2</b> )
Comp.	<b>82.5</b>	79.9 ( <b>-2.6</b> )
AA	<b>72.5</b>	69.5 ( <b>-3.0</b> )
<b>RSIVQA</b>		
Yes/No	<b>93.1</b>	88.7 ( <b>-4.4</b> )
Num.	<b>61.5</b>	56.1 ( <b>-5.4</b> )
Other	<b>89.0</b>	84.7 ( <b>-4.3</b> )
AA	<b>81.2</b>	76.5 ( <b>-4.7</b> )

the semantic continuity required for object recognition. Conversely, for the RSVQA-HR dataset, which features high-resolution imagery ( $512 \times 512$ ), the optimal configuration shifts to  $N = 16$  (a  $4 \times 4$  grid). Here, a coarser partition ( $N = 4$ ) fails to capture the fine-grained spatial nuances of small, densely distributed objects, while a finer partition ( $N = 16$ ) effectively isolates relevant regions. However, increasing  $N$  beyond this point again degrades performance, suggesting that over-segmentation introduces noise and hinders the model's ability to aggregate global context. Consequently, we adopt  $N = 4$  for LR/RSIVQA and  $N = 16$  for HR in our main experiments to ensure optimal structural alignment.

**Question-guided Sparse Fusion.** Table IV shows that replacing the question-guided sparse fusion with uniform prompts (i.e., assigning equal weights to all block-wise prompts when forming  $p_{\text{global}}$ ) consistently reduces accuracy across all datasets, with overall drops of 3.0–4.7 points. The degradation becomes more pronounced on Counting, Area, and Number questions, which demand precise localization and selective aggregation of spatial evidence. Uniform prompting assigns equal contributions to all spatial blocks, so background-dominated regions inject irrelevant cues into the global prompt. In contrast, GRASP conditions the fusion weights on the input question and sparsifies the aggrega-

tion, which suppresses irrelevant regions and concentrates capacity on query-relevant areas. These results indicate that GRASP improves RSVQA not only by introducing block-wise prompts, but by enabling query-dependent spatial selection that supports robust reasoning in cluttered RS scenes.

**Effect of Entmax Sparsity Parameter.** We analyze the impact of the Entmax sparsity parameter  $\alpha$ , which governs the density of the attention distribution during prompt fusion. As Table III presents, the model performance exhibits an inverted U-shaped trend as  $\alpha$  increases from 1.0 to 2.0 across all three datasets. The standard Softmax function ( $\alpha = 1.0$ ) yields the lowest performance (e.g., 65.9% AA on RSVQA-LR), primarily because it assigns non-zero probabilities to all spatial regions. This forces the model to incorporate irrelevant background noise, which is particularly detrimental in complex RS scenes. Increasing  $\alpha$  introduces necessary sparsity, which effectively filters out these distractions.

Performance peaks at  $\alpha = 1.5$ , where the model achieves the highest accuracy on all benchmarks (69.2%, 72.5%, and 81.2% AA, respectively). This suggests that  $\alpha = 1.5$  strikes an optimal balance, enabling the model to focus on salient regions while retaining sufficient contextual information. However, further increasing  $\alpha$  to 2.0 (Sparsemax) leads to a performance decline. This indicates that excessive sparsity causes the model to discard potentially useful peripheral context, resulting in information loss. Consequently, we select  $\alpha = 1.5$  as the default setting to ensure robust noise suppression without compromising semantic completeness.

## V. CONCLUSION

This paper demonstrates that explicitly modeling spatial structure plays a critical role in adapting general-purpose multimodal large language models to the RS domain. Our observations indicate that adaptation performance does not solely depend on parameter scale or tuning strategies, but is largely influenced by how visual information is spatially organized and queried. The performance of GRASP suggests that lightweight prompting mechanisms with spatial awareness can effectively compensate for the limitations of global adaptation strategies in complex scenes, providing a viable path toward parameter-efficient model transfer. Looking ahead, future work may explore more flexible region modeling to address the limitations of fixed grid partitioning, and extend spatially explicit prompting to temporal or multi-view RS data to improve spatiotemporal consistency.

## VI. ACKNOWLEDGEMENT

This work was supported by the National Natural Science Foundation of China (Grant No. 62572104).

## REFERENCES

- [1] S. Lobry, D. Marcos, J. Murray, and D. Tuia, “Rsvqa: Visual question answering for remote sensing data,” *IEEE Transactions on Geoscience and Remote Sensing*, vol. 58, no. 12, pp. 8555–8566, 2020.
- [2] Z. Huang, H. Yan, Q. Zhan, S. Yang, M. Zhang, C. Zhang, Y. Lei, Z. Liu, Q. Liu, and Y. Wang, “A survey on remote sensing foundation models: From vision to multimodality,” *arXiv preprint arXiv:2503.22081*, 2025.
- [3] X. Li, C. Wen, Y. Hu, Z. Yuan, and X. X. Zhu, “Vision-language models in remote sensing: Current progress and future trends,” *IEEE Geoscience and Remote Sensing Magazine*, 2024.
- [4] L. Gómez-Chova, D. Tuia, G. Moser, and G. Camps-Valls, “Multimodal classification of remote sensing images: A review and future directions,” *Proceedings of the IEEE*, vol. 103, no. 9, pp. 1560–1584, 2015.
- [5] Y. Zhang, P. Zheng, C. Zeng, B. Xiao, Z. Li, and X. Gao, “Jointly rs image deblurring and super-resolution with adjustable-kernel and multi-domain attention,” *IEEE Transactions on Geoscience and Remote Sensing*, 2024.
- [6] P. Zheng, J. Jiang, Y. Zhang, C. Zeng, C. Qin, and Z. Li, “Cgc-net: A context-guided constrained network for remote-sensing image super resolution,” *Remote Sensing*, vol. 15, no. 12, p. 3171, 2023.
- [7] F. Liu, D. Chen, Z. Guan, X. Zhou, J. Zhu, Q. Ye, L. Fu, and J. Zhou, “Remoteclip: A vision language foundation model for remote sensing,” *IEEE Transactions on Geoscience and Remote Sensing*, 2024.
- [8] Y. Zhou, L. Feng, Y. Ke, X. Jiang, J. Yan, X. Yang, and W. Zhang, “Towards vision-language geo-foundation model: A survey,” *arXiv preprint arXiv:2406.09385*, 2024.
- [9] K. He, X. Zhang, S. Ren, and J. Sun, “Deep residual learning for image recognition,” in *Proceedings of the IEEE conference on computer vision and pattern recognition*, 2016, pp. 770–778.
- [10] C. Chappuis, V. Zermatten, S. Lobry, B. Le Saux, and D. Tuia, “Prompt-rsvqa: Prompting visual context to a language model for remote sensing visual question answering,” in *Proceedings of the IEEE/CVF conference on computer vision and pattern recognition*, 2022, pp. 1372–1381.
- [11] L. Hackel, K. N. Clasen, M. Ravanbakhsh, and B. Demir, “Lit-4-rsvqa: Lightweight transformer-based visual question answering in remote sensing,” in *IGARSS 2023-2023 IEEE International Geoscience and Remote Sensing Symposium*. IEEE, 2023, pp. 2231–2234.
- [12] J. Songara, S. Pande, S. Choudhury, B. Banerjee, and R. Velmurugan, “Visual question answering in remote sensing with cross-attention and multimodal information bottleneck,” in *IGARSS 2023-2023 IEEE International Geoscience and Remote Sensing Symposium*. IEEE, 2023, pp. 6278–6281.
- [13] S. Siripong, A. Chaiyapan, and T. Phonchai, “Large vision-language models for remote sensing visual question answering,” *arXiv preprint arXiv:2411.10857*, 2024.
- [14] W. Zhang, M. Cai, T. Zhang, Y. Zhuang, J. Li, and X. Mao, “Earthmarker: A visual prompting multi-modal large language model for remote sensing,” *IEEE Transactions on Geoscience and Remote Sensing*, 2024.
- [15] A. Xiao, W. Xuan, J. Wang, J. Huang, D. Tao, S. Lu, and N. Yokoya, “Foundation models for remote sensing and earth observation: A survey,” *IEEE Geoscience and Remote Sensing Magazine*, 2025.
- [16] H. Li, X. Zhang, and H. Qu, “Ddfav: Remote sensing large vision language models dataset and evaluation benchmark,” *Remote Sensing*, vol. 17, no. 4, p. 719, 2025.
- [17] G.-S. Xia, X. Bai, J. Ding, Z. Zhu, S. Belongie, J. Luo, M. Datcu, M. Pelillo, and L. Zhang, “Dota: A large-scale dataset for object detection in aerial images,” in *Proceedings of the IEEE conference on computer vision and pattern recognition*, 2018, pp. 3974–3983.
- [18] S. Lobry and D. Tuia, “Visual question answering on remote sensing images,” in *Advances in Machine Learning and Image Analysis for GeoAI*. Elsevier, 2024, pp. 237–254.
- [19] X. X. Zhu, D. Tuia, L. Mou, G.-S. Xia, L. Zhang, F. Xu, and F. Fraundorfer, “Deep learning in remote sensing: A comprehensive review and list of resources,” *IEEE geoscience and remote sensing magazine*, vol. 5, no. 4, pp. 8–36, 2017.
- [20] Y. Bazi, L. Bashmal, M. M. Al Rahhal, R. Ricci, and F. Melgani, “Rslava: A large vision-language model for joint captioning and question answering in remote sensing imagery,” *Remote Sensing*, vol. 16, no. 9, p. 1477, 2024.
- [21] C. Pang, J. Wu, J. Li, Y. Liu, J. Sun, W. Li, X. Weng, S. Wang, L. Feng, G.-S. Xia *et al.*, “H2rsvlm: Towards helpful and honest remote sensing large vision language model,” *CoRR*, 2024.
- [22] Y. Zhan, Z. Xiong, and Y. Yuan, “Skyeyept: Unifying remote sensing vision-language tasks via instruction tuning with large language model,” *ISPRS Journal of Photogrammetry and Remote Sensing*, vol. 221, pp. 64–77, 2025.
- [23] E. J. Hu, Y. Shen, P. Wallis, Z. Allen-Zhu, Y. Li, S. Wang, L. Wang, W. Chen *et al.*, “Lora: Low-rank adaptation of large language models.” *ICLR*, vol. 1, no. 2, p. 3, 2022.
- [24] K. Kuckreja, M. S. Danish, M. Naseer, A. Das, S. Khan, and F. S. Khan, “Geochat: Grounded large vision-language model for remote sensing,” in *Proceedings of the IEEE/CVF Conference on Computer Vision and Pattern Recognition*, 2024, pp. 27831–27840.
- [25] W. Zhang, M. Cai, T. Zhang, Y. Zhuang, and X. Mao, “Earthgpt: A universal multimodal large language model for multisensor image comprehension in remote sensing domain,” *IEEE Transactions on Geoscience and Remote Sensing*, vol. 62, pp. 1–20, 2024.
- [26] D. Muhtar, Z. Li, F. Gu, X. Zhang, and P. Xiao, “Lhrs-bot: Empowering remote sensing with vgi-enhanced large multimodal language model,” in *European Conference on Computer Vision*. Springer, 2024, pp. 440–457.
- [27] S. Park, Y. Kim, S. Y. Kim, and Y. M. Ro, “Remote sensing large vision-language model: Semantic-augmented multi-level alignment and semantic-aware expert modeling,” *arXiv preprint arXiv:2506.21863*, 2025.
- [28] Z. Yuan, W. Zhang, K. Fu, X. Li, C. Deng, H. Wang, and X. Sun, “Exploring a fine-grained multiscale method for cross-modal remote sensing image retrieval,” *arXiv preprint arXiv:2204.09868*, 2022.
- [29] X. Zheng, B. Wang, X. Du, and X. Lu, “Mutual attention inception network for remote sensing visual question answering,” *IEEE Transactions on Geoscience and Remote Sensing*, vol. 60, pp. 1–14, 2021.
- [30] S. Antol, A. Agrawal, J. Lu, M. Mitchell, D. Batra, C. L. Zitnick, and D. Parikh, “Vqa: Visual question answering,” in *Proceedings of the IEEE international conference on computer vision*, 2015, pp. 2425–2433.
- [31] K. Xu, J. Ba, R. Kiros, K. Cho, A. Courville, R. Salakhudinov, R. Zemel, and Y. Bengio, “Show, attend and tell: Neural image caption generation with visual attention,” in *International conference on machine learning*. PMLR, 2015, pp. 2048–2057.
- [32] J. D. Silva, J. Magalhães, D. Tuia, and B. Martins, “Remote sensing visual question answering with a self-attention multi-modal encoder,” in *Proceedings of the 5th ACM SIGSPATIAL International Workshop on AI for Geographic Knowledge Discovery*, 2022, pp. 40–49.
- [33] J. Lu, D. Batra, D. Parikh, and S. Lee, “Vilbert: Pretraining task-agnostic visiolinguistic representations for vision-and-language tasks,” *Advances in neural information processing systems*, vol. 32, 2019.
- [34] J. Feng and H. Wang, “A multi-scale contextual attention network for remote sensing visual question answering,” *International Journal of Applied Earth Observation and Geoinformation*, vol. 126, p. 103641, 2024.
- [35] X. Sun, B. Peng, C. Zhang, F. Jin, Q. Niu, J. Liu, K. Chen, M. Li, P. Feng, Z. Bi *et al.*, “From pixels to prose: Advancing multi-modal language models for remote sensing,” *arXiv preprint arXiv:2411.05826*, 2024.
- [36] W. Zhang, M. Cai, Y. Ning, T. Zhang, Y. Zhuang, S. Lu, H. Chen, J. Li, and X. Mao, “Earthgpt-x: A spatial mllm for multi-level multi-source remote sensing imagery understanding with visual prompting,” *IEEE Transactions on Geoscience and Remote Sensing*, 2025.
- [37] T. Siebert, K. N. Clasen, M. Ravanbakhsh, and B. Demir, “Multi-modal fusion transformer for visual question answering in remote sensing,” in *Image and Signal Processing for Remote Sensing XXVIII*, vol. 12267. SPIE, 2022, pp. 162–170.
- [38] J. Wang, Z. Zheng, Z. Chen, A. Ma, and Y. Zhong, “Earthvqa: Towards queryable earth via relational reasoning-based remote sensing visual question answering,” in *Proceedings of the AAAI Conference on Artificial Intelligence*, vol. 38, no. 6, 2024, pp. 5481–5489.
- [39] D. Zhang, Y. Yu, J. Dong, C. Li, D. Su, C. Chu, and D. Yu, “Mm-lmms: Recent advances in multimodal large language models,” *arXiv preprint arXiv:2401.13601*, 2024.
- [40] S. Yin, C. Fu, S. Zhao, K. Li, X. Sun, T. Xu, and E. Chen, “A survey on multimodal large language models,” *National Science Review*, vol. 11, no. 12, p. nwae403, 2024.
- [41] H. Liu, C. Li, Y. Li, and Y. J. Lee, “Improved baselines with visual instruction tuning,” in *Proceedings of the IEEE/CVF conference on computer vision and pattern recognition*, 2024, pp. 26296–26306.
- [42] P. Wang, S. Bai, S. Tan, S. Wang, Z. Fan, J. Bai, K. Chen, X. Liu, J. Wang, W. Ge *et al.*, “Qwen2-vl: Enhancing vision-language

model's perception of the world at any resolution," *arXiv preprint arXiv:2409.12191*, 2024.

[43] N. Houlsby, A. Giurgiu, S. Jastrzebski, B. Morrone, Q. De Laroussilhe, A. Gesmundo, M. Attariyan, and S. Gelly, "Parameter-efficient transfer learning for nlp," in *International conference on machine learning*. PMLR, 2019, pp. 2790–2799.

[44] B. Lester, R. Al-Rfou, and N. Constant, "The power of scale for parameter-efficient prompt tuning," *arXiv preprint arXiv:2104.08691*, 2021.

[45] K. Zhou, J. Yang, C. C. Loy, and Z. Liu, "Learning to prompt for vision-language models," *International Journal of Computer Vision*, vol. 130, no. 9, pp. 2337–2348, 2022.

[46] Zhou, Kaiyang and Yang, Jingkang and Loy, Chen Change and Liu, Ziwei, "Conditional prompt learning for vision-language models," in *Proceedings of the IEEE/CVF conference on computer vision and pattern recognition*, 2022, pp. 16 816–16 825.

[47] M. Jia, L. Tang, B.-C. Chen, C. Cardie, S. Belongie, B. Hariharan, and S.-N. Lim, "Visual prompt tuning," in *European conference on computer vision*. Springer, 2022, pp. 709–727.

[48] Q. Wang, Y. Mao, J. Wang, H. Yu, S. Nie, S. Wang, F. Feng, L. Huang, X. Quan, Z. Xu *et al.*, "Aprompt: Attention prompt tuning for efficient adaptation of pre-trained language models," in *Proceedings of the 2023 conference on empirical methods in natural language processing*, 2023, pp. 9147–9160.

[49] A. Bhattacharya, M. Singha, A. Jha, and B. Banerjee, "C-saw: self-supervised prompt learning for image generalization in remote sensing," in *Proceedings of the Fourteenth Indian Conference on Computer Vision, Graphics and Image Processing*, 2023, pp. 1–10.

[50] J. Zhu, Y. Li, K. Yang, N. Guan, Z. Fan, C. Qiu, and X. Yi, "Mvp: Meta visual prompt tuning for few-shot remote sensing image scene classification," *IEEE Transactions on Geoscience and Remote Sensing*, vol. 62, pp. 1–13, 2024.

[51] B. Peters, V. Niculae, and A. F. Martins, "Sparse sequence-to-sequence models," *arXiv preprint arXiv:1905.05702*, 2019.

[52] H. Liu, C. Li, Y. Li, B. Li, Y. Zhang, S. Shen, and Y. J. Lee, "Llava-next: Improved reasoning, ocr, and world knowledge," January 2024. [Online]. Available: <https://llava-vl.github.io/blog/2024-01-30-llava-next/>

[53] S. Bai, K. Chen, X. Liu, J. Wang, W. Ge, S. Song, K. Dang, P. Wang, S. Wang, J. Tang *et al.*, "Qwen2. 5-vl technical report," *arXiv preprint arXiv:2502.13923*, 2025.

[54] S.-Y. Liu, C.-Y. Wang, H. Yin, P. Molchanov, Y.-C. F. Wang, K.-T. Cheng, and M.-H. Chen, "Dora: Weight-decomposed low-rank adaptation," in *Forty-first International Conference on Machine Learning*, 2024.